Prediction of loess soil-water characteristic curve by mercury intrusion porosimetry

LI Hua[1] https://orcid.org/0000-0002-7468-6573; e-mail: hual16@163.com

LI Tong-lu[1,2]* https://orcid.org/0000-0001-6561-1871; ✉ e-mail: dcdgx08@chd.edu.cn

LI Ping[1,2] https://orcid.org/0000-0002-6010-961X; e-mail: dcdgx07@chd.edu.cn

ZHANG Ya-guo[2,3] https://orcid.org/0000-0002-9739-715X; e-mail: yaguozhang29@chd.edu.cn

*Corresponding author

1 Department of Geological Engineering, Chang'an University, Xi'an 710054, China

2 Observation and Research Station for the Chinese Loess Plateau, Ministry of Education, Zhengning 745399, China

3 Department of Civil Engineering, Chang'an University, Xi'an 710054, China

Citation: Li H, Li TL, Li P, Zhang YG (2020) Prediction of loess soil-water characteristic curve by mercury intrusion porosimetry. Journal of Mountain Science 17(9). https://doi.org/10.1007/s11629-019-5929-2

Abstract: Mercury intrusion porosimetry (MIP) is a simple and fast way to obtain the pore distribution of soil and can be used to estimate the soil-water characteristic curve (SWCC). In previous studies, soil was assumed to be a perfect wettability material, and the contact angle (CA) of the soil-water interface was taken as zero in the SWCC prediction method. However, the CA has proved to be much greater than zero even for hydrophilic soils according to some soil wettability experiments, and it has a significant effect on predicting the SWCC. In this research, a method for predicting the SWCC by MIP, which takes the CA as a fitting coefficient, is proposed. The pore size distribution curves are measured by MIP, and the SWCCs of two loess soils are measured by pressure plate and filter paper tests. When the CA is taken as 70° and 50° for the wetting and drying process, respectively, the SWCCs predicted by the pore size distribution curves agree well with the measured SWCCs. The predicted suction range of the proposed method is 0-10^5 kPa. The consistency of the results suggests that utilizing the MIP test to predict the SWCC with a proper CA is effective for loess.

Notation

Symbol	Explanation
CA	Contact angle
CRM	Capillary rising method
FPT	Filter paper test
MIP	Mercury intrusion porosimetry
PPT	Pressure plate test
PSD	Pore size distribution
SDM	Sessile drop method
SWCC	Soil-water characteristic curve
WPM	Wilhelmy plate method
d	Pore diameter
m_h	Slope of the w^2 - t curves of n-hexane
m_w	Slope of the w^2 - t curves of water
n	Porosity of the sample
P_m	Intruding pressure of MIP
T_m	Surface tension of the mercury phase
T_w	Surface tension of the water phase
V_a	Real air volume
$V_{a,m}$	Air volume measured with MIP
V_m	Mercury volume
V_{max}	Nondetected pore volume (pores that are too large to measure with MIP)

V_{min}	Nonintruded pore volume (pores are too small for mercury to intrude with MIP)
V_s	Soil solid volume
V_t	Real total soil volume
$V_{t,m}$	Total soil volume measured by MIP
V_w	Intruded water volume
w	Increased mass at CRM test
α_m	Contact angle at the air-mercury-soil interface
α_w	Contact angle at the air-water-soil interface
α_{wd}	Drying contact angle at the air-water-soil interface
α_{ww}	Wetting contact angle at the air-water-soil interface
η_h	Dynamic viscosity of n-hexane
η_w	Dynamic viscosity of water
θ_w	Volumetric water content
ρ_d	Real soil density
$\rho_{d,m}$	Soil density measured by MIP
ρ_h	Density of n-hexane
ρ_w	Density of water
$\sigma_{lv,h}$	Surface energy of n-hexane
$\sigma_{lv,w}$	Surface energy of water
ψ	Matric suction

Introduction

Water in loess can induce failure of microstructures and thereby induce ground collapse, uneven settlement, and slope sliding (Li et al. 2016; Xie et al. 2018). Thus, the soil-water characteristic curve (SWCC) of loess plays an important role in the design of geotechnical infrastructure. The measurement of the SWCC is time consuming because it is mostly based on the equilibrium of the pore-water pressure in the soil with the imposed matric suction in the measuring system or the stabilization of variables that are sensitive to changes in water content (Masrouri et al. 2008; Wang et al. 2015; Li et al. 2016). Therefore, approaches to determine SWCCs via other soil properties (such as the dry density, grain size distribution, and pore size distribution (PSD)) have been investigated by many researchers (Ng et al. 2016; Li et al. 2018; Ye et al. 2019). The PSD measured by mercury intrusion porosimetry (MIP) is a simple method used to predict the SWCC (Diamond 1970; Romero and Simms 2008; Zhang and Li 2010).

Prapaharan et al. (1985) first proposed a method to evaluate the SWCC by assuming that the mercury intrusion path is equivalent to the moisture desorption of unsaturated soil. They suggested that the prediction at low suction (<10 kPa) is better than that at high suction (10-10³ kPa).

Many researchers have since investigated the method with different soil materials and proposed available conditions for application. Romero et al. (1999) considered the residual water that is adsorbed to the particle surface and predicted the SWCCs of two compacted clays within the suction range of 0.01~4.5×10⁴ kPa. Although they assimilated the mercury intrusion procedure to the desorption path, the predicted SWCCs correspond more to the measured wetting curves. Simms and Yanful (2001a, 2001b) used MIP to measure the PSDs of compacted plastic soils before and after SWCC testing. They demonstrated that pores shrink during the SWCC test, large pores connected to small pores can become trapped during drainage, and water may be isolated by the non-wetting phase. However, the actual volume of the pores that shrink and are trapped and isolated during the SWCC test is difficult to determine. Zhang and Li (2010) stated that the MIP method is appropriate for only a limited pore size range because pores beyond 0.003-73 μm cannot be detected by MIP. Their prediction for fine soil seemed better than that for coarse soil. Romero and Simms (2008) concluded that the prediction from MIP is limited to low suction, where the capillary water dominates the water retention. Simms and Yanful (2005) estimated the SWCC by establishing a pore network model with hydromechanical coupling using the initial microstructure measured by MIP. However, all these methods simply took the CA as zero and did not consider the effect of the CA. In fact, the CA is greater than zero even for hydrophilic soils (Hajnos et al. 2013), and it has a significant effect on the SWCC (Liu et al. 2013b). Moreover, these past studies were rarely concerned with loess. It is necessary to verify whether the MIP test is available for loess, and an elaborate prediction method for loess is required.

Loess is a windblown deposit during the glacial period under a semiarid to arid climate (Feda 1988; Sun 2005). It is widely agreed that loess soil consists of grains typically from 10 to 60 μm, and grains larger than 20 μm account for approximately 75% of the solids (Tan 1988; Dijkstra et al. 1994; Li et al. 2016). The primary grains together with the aggregates (primary grains coated by clay platelets or calcium carbonate) constitute the skeleton of the loess (Gao 1979, 1980). With these components, loess is typically

formed with a high porosity, a loose honeycomb-type structure, and open pores (Sun 2005; Gao 1980; Muñoz-Castelblanco et al. 2012; Li et al. 2016). This structure leads to a better connectivity than other fine soils, allowing mercury to more easily intrude into the most pores in loess in MIP tests (Muñoz-Castelblanco et al. 2012). These characteristics provide a great possibility to establish a good prediction of the SWCC of loess with MIP tests.

However, the CA of loess has hardly been measured. The CA of soils varies with the content of organic material, the soil mineralogical composition, and the particle size distribution (Woche et al. 2005). The CAs of agricultural and forest soils measured by Woche et al. (2005) range from 0° to 130° for different soil types. The CAs measured by Bachmann et al. (2003) range from 40° to 140° and 0° to 80° for advancing and receding CAs of different soils, respectively. These values indicate the large variation of the CAs of different soils, and therefore, the CA of loess is an essential parameter in our research.
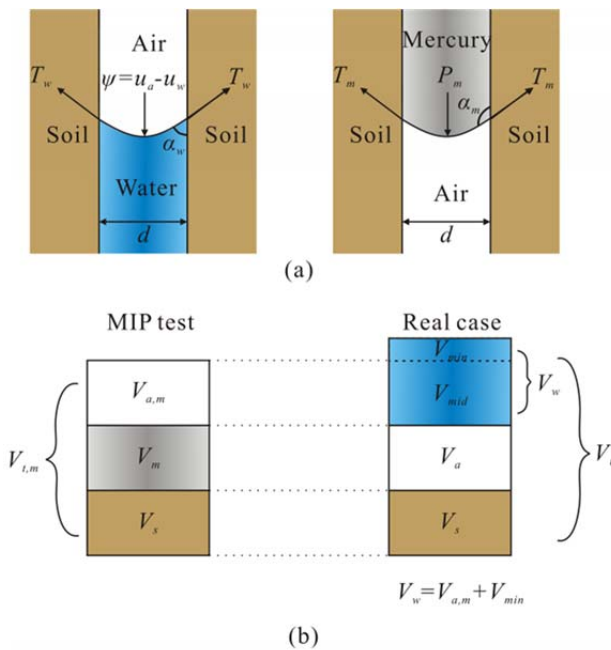
Figure 1 Schematic diagrams of water retention characteristics and mercury retention in soil (a) and the proportions of the three phases measured with the mercury intrusion porosimetry (MIP) test and in the real case (b).

In this paper, a method for predicting the SWCC by MIP, in which the CA is taken as a fitting coefficient that correlates to the loess soil properties, is proposed. The PSDs of two loess soils

from the China Loess Plateau were measured by the MIP test, and the SWCCs were measured by the pressure plate method combined with the filter paper method for comparison. The available CAs for loess are obtained by fitting the predicted SWCC to the measured SWCC and verified with the capillary rising test.

1 Prediction Method

The proposed prediction method is based on the hypothesis that the soil pores are ideal cylindrical channels and water is stored in pores as capillary water. Figure 1a shows the schematic diagrams of an air-water-soil interface and an air-mercury-soil interface. Based on the force equilibrium on the interface (Figure 1a), a relationship between the matric suction (air pressure minus water pressure) and the surface tension on the water phase has been built, which is the classical Young-Laplace equation:

$$\psi = \frac{4T_w \cos \alpha_w}{d} \tag{1}$$

where ψ is the matric suction; T_w is the surface tension of the water phase, T_w=72.75×10^{-3} N/m at 20°C; α_w is the CA at the air-water-soil interface (Figure 1a), and α_w=0°-90°; and d is the equivalent pore diameter at a specific matric suction ψ.

Mercury intrusion into porous materials follows similar principles, as expressed by Washburn (1921), which also assume that the pore shape is an ideal cylindrical channel (Figure 1a). The Washburn equation is expressed as

$$P_m = -\frac{4T_m \cos \alpha_m}{d} \tag{2}$$

where P_m is the intruding pressure applied to the mercury; T_m is the surface tension of the mercury phase, T_w=485×10^{-3} N/m at 20°C, α_m is the CA at the air-mercury-soil interface (Figure 1a), and α_m=130°, because 130° is a common used value for soil in the MIP test, and the value usually varies between 130° and 140° for soil (Lu and Licos 2004; Romero and Simms 2008); and d is the equivalent pore diameter at a specific intruding pressure P_m.

For fluid intrusion into pores with the same pore diameter radius d, the two equations can be related to obtain the corresponding matric suction:

$$\psi(d) = -P_m \frac{T_w \cos\alpha_w}{T_m \cos\alpha_m} \qquad (3)$$

Figure 1a shows schematic diagrams of the water retention characteristics and mercury intrusion in a soil. The CAs of mercury and water are different. Water and mercury intrude into the pores in opposite ways. Water prefers to fill small pores first, while mercury prefers large pores. The matric suction decreases during soil wetting, and high matric suction occurs in small capillary tubes. Thus, the water first occupies fine pores with high matric suction during the wetting process. However, mercury more easily intrudes into larger pores under an applied external pressure P_m. Therefore, the water-occupied space and the mercury-occupied space are complementary. The intruded water volume V_w that correlates to a definite pore diameter can be calculated by subtracting the intruded mercury volume V_m from the total void volume.

However, the MIP test may underestimate the void volume of the soil if there are nonintruded pores and nondetected pores in the specimen, as mentioned before. The MIP device used in this research can measure pores with a size of 0.001-350 μm. Therefore, the total pore space of a soil specimen includes three parts: 1) The nonintruded pore volume V_{min} (<0.01 μm) of pores that are too small for mercury to intrude into (these pores commonly exist in soils with a high clay content); 2) the intruded cumulative volume measured by MIP $V_{t,m}$ (0.001-350 μm); 3) the nondetected pore volume V_{max} (>350 μm) of pores that are too large to be measured under the pressures applied during the MIP process.

Lei (1987) classified loess pores into original pores (i.e., intragranular pores (<2 μm) and intergranular pores (2-32 μm)) and secondary pores (i.e., root holes, wormholes, mouse holes, joints, and fissures, (>32 μm)) (Li et al. 2016). Intergranular pores account for the majority of the pores in soil, intragranular pores form a minor portion, and secondary pores rarely exist in loess (they are commonly found at shallow depths of loess plateaus, within approximately 1.0 m) (Lei 1983). Therefore, nondetected pores (<0.01 μm) are ignored for loess; i.e., V_{max}=0. Figure 1b shows the proportions of the three phases measured with the MIP test compared to those of the real case.

$V_{t,m}$ and $V_{a,m}$ are the total specimen volume and the air volume measured with MIP, respectively; V_t and V_a are the real total specimen volume and the air volume, respectively. The soil solid volume V_s is the same in both cases. The mercury volume V_m equals the real air volume V_a. Because the nondetected pores V_{max} are ignored, the intruded water volume V_w is slightly larger than $V_{a,m}$, and $V_w = V_{a,m}+V_{min}$.

The volume water content of the soil is expressed as

$$\theta_w = n - \frac{V_m}{V_t} \qquad (4)$$

However, the dry density, $\rho_{d,m}$, measured by the MIP test does not match the real case. The total specimen volume $V_{t,m}$ is derived from the mercury volume, which fills the space around the sample in the sample chamber at the beginning of the MIP test. The mass m of the specimen is also measured at the beginning of the test. Therefore, $\rho_{d,m}$ is calculated by dividing $V_{t,m}$ by m. Additionally, the intruded mercury volume V_m is measured during the MIP test. Therefore, the water content is calculated by

$$\theta_w = n - \frac{V_m}{V_{t,m}} \times \frac{\rho_d}{\rho_{d,m}} \qquad (5)$$

In addition, V_m can be expressed by the integral of the pore distribution curve:

$$V_m = \int_{d(\psi)}^{d_{max}} f(d)dd \qquad (6)$$

where $d(\psi)$ is the intruding pore corresponding to suction ψ, d_{max} is the maximum pore diameter, and $f(d)$ is the probability distribution of pores.

The SWCC is then obtained by correlating the matric suction derived by Equation 3 and the water content derived by Equation 5.

The air-water-soil CA is an unknown parameter and should be determined in the proposed method. Figure 2 shows a conceptual model for the different CAs on the drying and wetting sides of a water drop flowing on an inclined solid surface. The wetting CA α_{ww} develops on the advancing edge of a flowing drop and is larger than the drying CA α_{wd}, which develops on the receding edge. The mechanism of this phenomenon is that the water attracted by soil particles exhausts less energy than the water escaping from soil particles.

This makes the difference of the CA an important reason for the hysteresis of the SWCC (different matric suctions at the same water content for drying and wetting conditions). Instead of the assumed zero, actual drying and wetting CAs, as shown in Figure 2, should be taken into Equation 1 to calculate the real SWCC.

Figure 3 plots the SWCCs under different CAs at 20°C. The matric suction and water content are calculated by Equation 3 and Equation 5, respectively, based on the proposed method. The parameters and PSD data are those of the Heifangtai loess and are provided below (Table 1; Figure 8). The larger the CA value, the larger the changes in the matric suction and, consequently, the greater the effect of the CA on the SWCC. Based on the SWCCs in Figure 3, the matric suction versus CA at water contents of 12%, 22%, and 45% is calculated by Equation 1 and shown in Figure 4. Figure 4 indicates that the lower the water content is, the more quickly the matric suction decreases as the CA increases. Therefore, the drier the soil, the greater the effect of the CA on the SWCC. In consideration of the CA, the hysteresis between the drying and wetting SWCCs can be derived.

The CA reflects the surface characteristics of a particle. Several methods have been developed to measure the CA. The capillary rising method (CRM), the Wilhelmy plate method (WPM), and the sessile drop method (SDM) are the most commonly used CA measuring methods. The CRM measures the advancing CA; the WPM measures the advancing, receding, and apparent CA; and the SDM measures the apparent CA. Woche et al.'s (2005) and Bachmann et al.'s (2003) measurements on different soils are based on these methods. Because loess has a similar texture to the silty clay in Bachmann et al.'s (2003) study, the advancing CA of loess might be approximately similar with that of silty clay (73.9° from the CRM but 49.2° from the WPM). Bachmann et al. (2003) and Shang et al. (2008) compared the measuring methods mentioned above and concluded that the measured CA largely varies (the difference ranged from 2° to 30° for Bachmann et al. (2003) and from 10° to 40° for Shang et al. (2008)) between different methods. Because remarkable deviations exist in the CA measurements between different methods, this paper regards the CA as a regression

coefficient for predicting the SWCC with the MIP method. In addition, the CRM is used to measure the CA of loess for comparison.
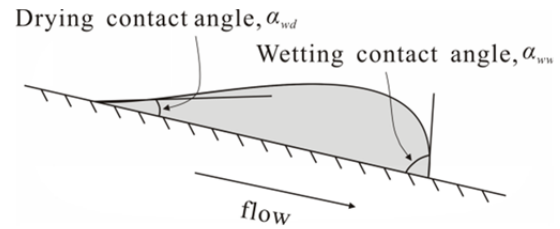

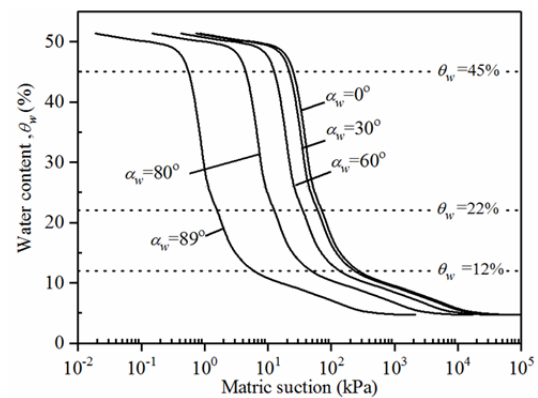**Figure 2** A flowing water drop illustrating the drying and wetting contact angles.

Figure 3 Soil-water characteristic curves under different contact angles (α_w).
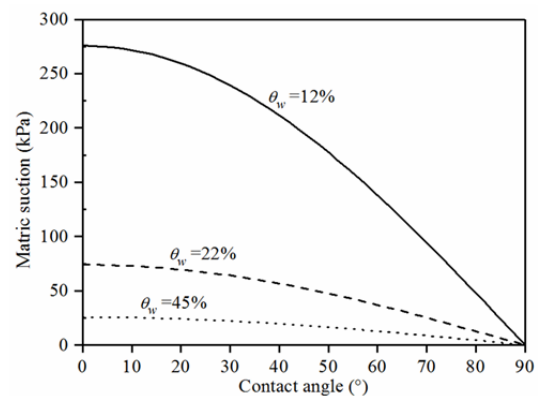

Figure 4 Matric suction variation with the contact angle at water contents (θ_w) of 12%, 22%, and 45%.

2 Experiments

The specimens were collected from the Malan loess (Late Pleistocene) in Heifangtai and Jingyang on the Chinese Loess Plateau (Figure 5). Heifangtai is in the west of the plateau (west of Liupan Mountain), and Jingyang is in the south (in the Wei River basin). Pressure plate tests (PPTs) and

filter paper tests (FPTs) were implemented to determine the SWCC, MIP was implemented to determine the PSD, and the CRM was implemented to measure the advancing CAs.

Figure 5 Sampling sites of the Heifangtai and Jingyang specimens.

2.1 Soil-Water Characteristic Curve Measurement

The PPT was used to measure low-suction SWCCs (0-600 kPa), and the FPT was used to measure high-suction SWCCs (600-10⁵ kPa).

The pressure plate used in this research was a Fredlund SWCC apparatus produced by GCTS Co., Ltd., with a 15 bar high air entry ceramic disk. Intact loess specimens within a mental ring were first saturated and then installed in the pressure plate for the drying process, with the pressure increasing from 0 kPa to 600 kPa. Once the drying process finished, the matric suction was decreased gradually from 600 kPa to 0 kPa to derive the wetting SWCC. The matric suction and water quantity flowing out were recorded during the entire test to derive the SWCCs. The FPT could measure the SWCC only between the drying and wetting curves rather than the main drying and wetting curves (Sun et al. 2013). The filter paper employed was Whatman No. 42. Several pairs of intact soil samples were dripped into different water contents, with three filter papers sandwiched in the middle of the two samples. The middle filter paper was used to determine the matric suction, and the other two were larger than the middle one to prevent it from being contaminated. The entire system was wrapped with silver paper and then wax-sealed and placed into a sealed glass container.

After 15 days at 20℃, the soil samples and filter papers were removed and weighed to determine the water content and matric suction. The matric suction was estimated through a predetermined calibration curve of filter paper according to ASTM D5298-10 2013:

$$\lg \psi = \begin{cases} 5.327 - 0.0779 w_{fp} & w_{fp} < 45.3\% \\ 2.412 - 0.0135 w_{fp} & w_{fp} > 45.3\% \end{cases} \quad (7)$$

where ψ is the soil matric suction, and w_{fp} is the measured gravimetric water content of the filter paper.

2.2 Mercury Intrusion Porosimetry Test

The two loess specimens were tested via MIP to derive their PSDs. The specimens were cut into small cylinders that were 1 cm in diameter and 1.5 cm in height for the MIP test. Before testing, the specimens were subjected to a freeze-drying process to eject the water from the pores. In the freeze-drying process, instantaneous freezing was utilized to minimize shrinkage while drying to avoid soil structure changes (Romero et al. 1999). After the freeze-drying process, an AutoPore IV 9500 porosimetry apparatus (USA, Micromeritics Instrument Corporation) was used to measure the pore size with regard to the mercury intrusion pressure. The mercury intrusion pressure ranged from 0 MPa to 418 MPa, while the measured pore diameters ranged from 0.001 μm to 350 μm. The applied pressure and intruded mercury volume were automatically recorded during the test.

2.3 Contact Angle Measurement

Research indicates several acceptable techniques to measure the advancing CA, but testing the receding CA of soil material can be challenging because of the difficulty of the technique and deviations in the results (Bachmann et al. 2003; Goebel et al. 2008, Shang et al. 2008). Therefore, the CRM was used to verify the value of the advancing CA.

The soil was air-dried and sieved. A glass tube, with a diameter of 1.5 cm, with filter paper on the bottom was filled with 20 g of soil. The tube was hung from an electric balance, which could measure the mass variation in the soil. A reservoir with a test liquid (either n-hexane or water) was

placed below the tube so that the liquid surface touched the bottom of the tube. As the mass of the tube increased, the increased mass w and time t were recorded to determine the CA. N-hexane was used as a complete wetting fluid (its CA was zero) for comparison, and the water-soil CA α_w based on Bachmann et al. (2003) is given as

$$\cos(\alpha_w) = \left[m_w \eta_w / (\sigma_{lv,w} \rho_w^2) \right] / \left[m_h \eta_h / (\sigma_{lv,h} \rho_h^2) \right] \quad (8)$$

where m_w and m_h are the slopes of the w^2-t curves of water and n-hexane, which are determined by the capillary rise test; η_w, $\sigma_{lv,w}$, and ρ_w are the dynamic viscosity, surface energy, and density of the water; η_h, $\sigma_{lv,h}$, and ρ_h are the dynamic viscosity, surface energy, and density of the n-hexane. Under a 20°C testing temperature, $\eta_w = 1.01 \times 10^{-3}$ N s/m², $\eta_h = 3.01 \times 10^{-4}$ N s/m², $\sigma_{lv,w} = 7.28 \times 10^{-2}$ N/m, $\sigma_{lv,h} = 1.84 \times 10^{-2}$ N/m, $\rho_w = 1000$ kg/m³, and $\rho_h = 659$ kg/m³.

3 Results Analysis

The specimens were first tested to measure the general physical properties and particle size composition. The results are listed in Table 1. The particle size distribution curves were determined by the Bettersize 2000 laser particle analyzer and are plotted in Figure 6. For the specimen sampled in Heifangtai, the clay fraction (<2 μm) accounts for 7.4%, while the silt fraction (2-50 μm) accounts for 78.3%. For the Jingyang sample, the clay fraction (<2 μm) accounts for 12.3%, while the silt fraction (2-50 μm) accounts for 71.0%. The loess in Heifangtai has a lower clay content than that of the loess in Jingyang.
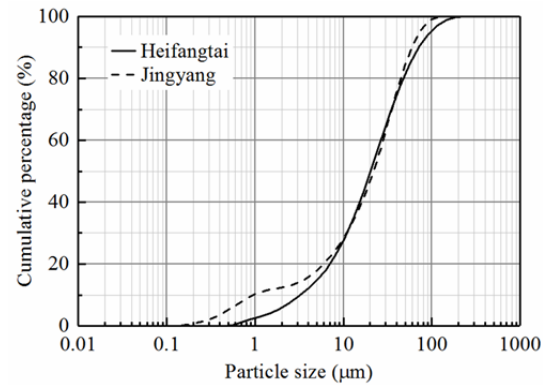
Figure 7 shows the cumulative intruded mercury volume V_m with respect to the applied pressure P_m during the MIP test. From these data, the PSD curves of the two soils (Figure 8) were derived. The intruded pore diameter was derived by the Washburn equation (Equation 2), where the CA at the air-mercury-soil interface was $\alpha_m = 130°$, and the surface tension of mercury was $T_m = 485 \times 10^{-3}$ N/m (at 20°). The pore size density—namely, the differential of the intruded mercury volume, $dV_m/d\log D$—was derived and is shown in Figure 8.

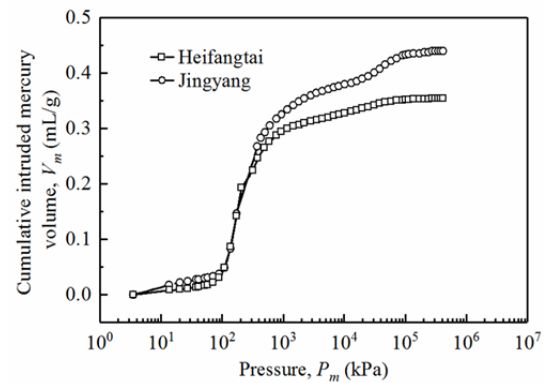The cumulative intruded mercury volume V_m in Figure 7 was used to calculate the water content

Table 1 Physical properties of the Heifangtai and Jingyang loess

| Specimen	$\rho_{d,m}$ (g/cm³)	ρ_d (g/cm³)	e	n
Heifangftai	1.30	1.32	1.04	0.51
Jingyang	1.26	1.22	1.22	0.55

Note: $\rho_{d,m}$, mercury intrusion porosimetry-measured dry density; ρ_d, dry density; e, void ratio; n, porosity.

Figure 6 Particle size distribution curves of Heifangtai and Jingyang loess.

Figure 7 Cumulative intruded mercury volume variation with applied pressure during the mercury intrusion porosimetry test.
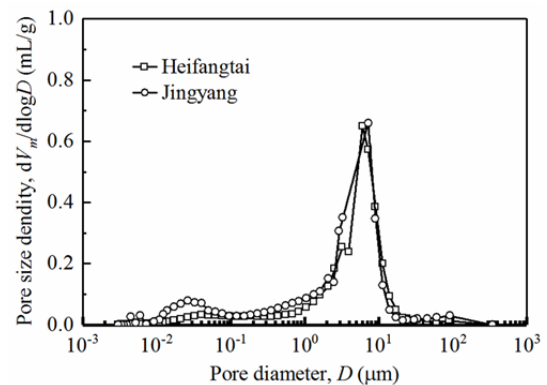

Figure 8 Particle size distribution curves measured by the mercury intrusion porosimetry test. V_m, intruded mercury volume.

with Equation 5. The applied pressure in Figure 7 was used to calculate the matric suction with Equation 3; the water surface tension was assumed to be T_w=72.75×10^{-3} N/m (at 20°). In Equation 3, the CA α_w is an uncertainty coefficient and has different values for wetting and drying cases. The α_w value for the calculated curves was adjusted to find the best fit to the PPT measuring points. Therefore, the α_w values were 70° in the wetting case and 50° in the drying case. The results are shown in Figure 9.

This result indicates that the predicted SWCCs are in good agreement with the PPT measured data in the suction range from 0 kPa to 600 kPa when the CAs are taken as 70° during the wetting process and 50° during the drying process. As the CA is taken as 0°, as in previous studies, the suction is overestimated by MIP data. At suctions higher than 600 kPa, the hysteresis between drying and wetting is not as obvious as that at low suctions, but the predicted SWCCs still show good agreement with the FPT-measured curves. The predicted curves show hysteresis in the high range, but the PPT curves show a convergence at 600 kPa. This result is due to the testing procedure of the PPT, in which the applied pressure was increased to 600 kPa and then decreased immediately for the same sample. Furthermore, the hysteresis for suctions higher than 600 kPa (lower than 10^5 kPa) for loess has been proved to exist (Muñoz-Castelblanco et al. 2012; Xie 2018; Fu 2018). Therefore, hysteresis for suctions larger than 600 kPa is very likely to exist.

Figure 10 shows the relationship between the square of the increased mass w^2 versus the time t during the capillary rise tests. The advancing CAs calculated from Equation 8 are 72.0° for the Heifangtai loess and 72.5° for the Jingyang loess, which corresponds to the adjusted value of 70° for
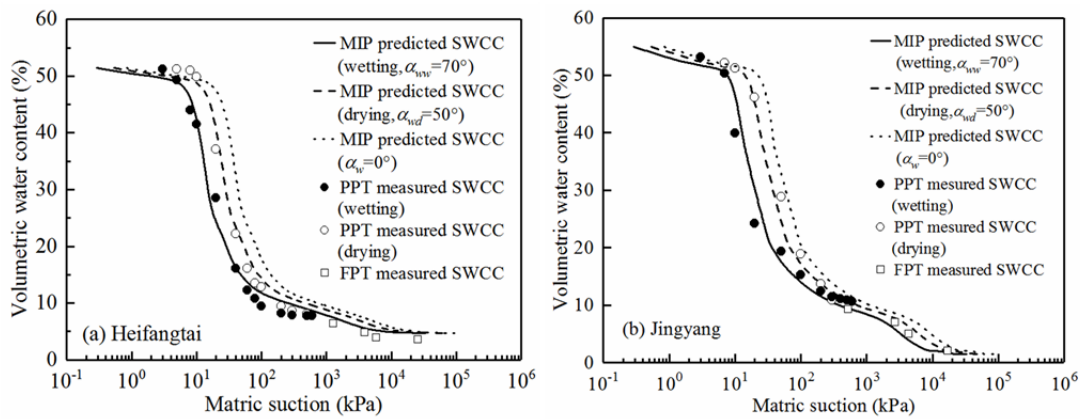
Figure 9 Predicted and measured soil-water characteristic curves of the Heifangtai (a) and Jingyang (b) loess

Note: SWCC, soil-water characteristic curve; MIP, mercury intrusion porosimetry; PPT, pressure plate test; FPT, filter paper test; α_w, contact angle; α_{ww}, wetting contact angle; α_{wd}, drying contact angle.
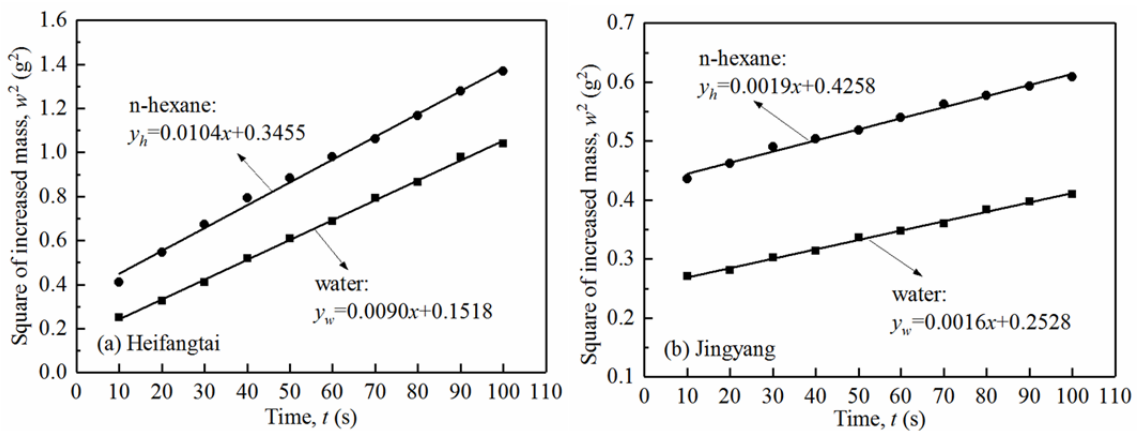
Figure 10 Square of the increased mass w^2 versus time t of the Heifangtai (a) and Jingyang (b) loess from the capillary rise tests.

these two types of loess.

Figure 9 also shows that the predicted SWCC of the Heifangtai soil has a single slope in the range from 10 to 10^2 kPa, resulting in a unimodal form. The Jingyang curve exhibits two slopes, from 10 to 10^2 kPa and from 10^3 to 10^4 kPa, resulting in a bimodal form. The slope under low suction is much steeper than that under high suction.

To analyze the effect of the PSD on the SWCC, the pore diameters are transformed to matric suction based on the Young-Laplace equation (Equation 1), with the CA a_w taken as 70° in the wetting case and 50° in the drying case. The new PSD curves and the corresponding SWCC are shown in Figure 11. For the Heifangtai loess, as shown in Figure 11a, the wetting SWCC shows a steep slope at $3-10^2$ kPa, and the corresponding PSD curve shows a peak in the same suction range. The highest pore density of the peak is 0.64 mL/g. This curve morphology is unimodal. For the Jingyang loess, as shown in Figure 11b, the wetting curve exhibits two peaks in the PSD curve. One peak appears at $3-10^2$ kPa and is extremely distinct, with the highest pore density of 0.66 mL/g. The other peak appears at $1\times10^3-7\times10^3$ kPa, with the highest pore density of 0.08 mL/g. These two peaks correspond to two steep slopes in the SWCC curve in the same suction range, and the first slope is steeper than the second. Apart from the sloped segments, the other parts of the SWCC are relatively flat. The two peaks or slopes refer to the bimodal form of the curve (Liu et al. 2013a). The difference between the Heifangtai loess and the Jingyang loess is related to the higher clay content in the Jingyang loess (Table 1). The main peak on the PSD curve for both soils is attributed to the intergranular pores, which accounts for most of the pores in loess. Soil with more clay grains such as the Jingyang loess shows a weak peak for small pores (0.01-0.1 μm in Figure 8), which is related to more intragranular pores that resulted from higher aggregate contents. This is why the PSD and SWCC of the Jingyang loess show bimodal forms.

The drying and wetting curves show a hysteresis in the matric suction for both the SWCC and the PSD. The good agreement between the predicted SWCCs and the measured data suggests that it is feasible to use a PSD curve to predict a loess SWCC by assuming an appropriate CA. In addition, MIP can derive SWCCs in the suction range of $0-10^5$ kPa.

4   Discussion

Wang et al. (2017) and Kuila and Prasad (2013) noted the limitation of the MIP test: MIP cannot measure the real pore volume at very high pressures (corresponding to the prediction of low suction values) because the sample may be compressed and new fissures may be created on the particles. Penumadu and Dean (2000) and Sills et al. (1973) concluded that no breakage or fracture occurs under high MIP pressures based on scanning electron micrographs (SEMs) and by comparing the PSDs derived from MIP and nitrogen-sorption techniques. The disagreement among the authors can be attributed to the different specimens used for testing. For soils with many enclosed pores or implicit fissures, the pressure in the specimen is not balanced under a sudden increase in mercury, and fissures or cracks may be created. For a soil with
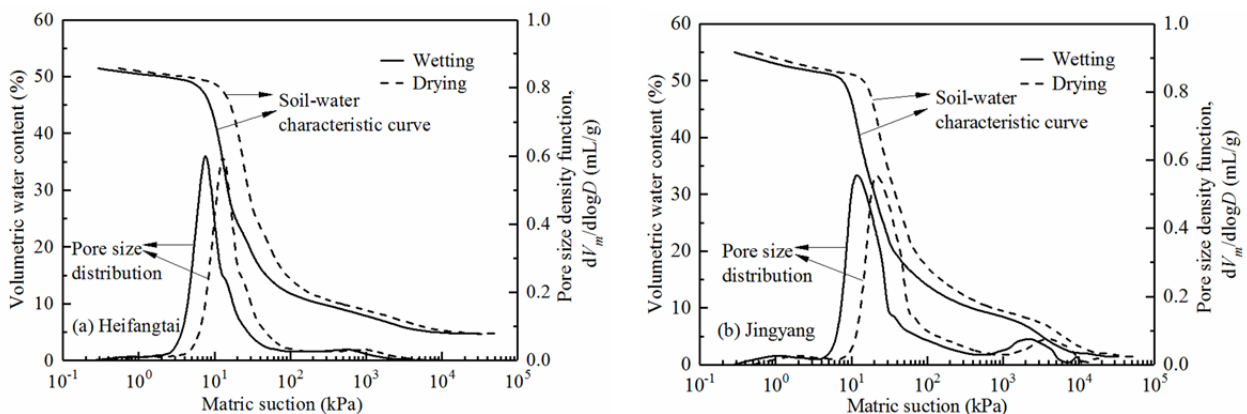
Figure 11 Predicted and measured soil-water characteristic curves of the Heifangtai (a) and Jingyang (b) loess. *D*, pore diameter; V_m, intruded mercury volume.

open and connected pores such as loess, fissures will not be created, and MIP is available; therefore, the prediction is also available.

The pore distribution during the drying and wetting processes was assumed to be invariable, and wetting-induced collapse and drying-induced shrinkage in soil (Ng et al. 2016) were ignored in the prediction method. The deformation of the soil or changes of the pores entail another complicated problem of unsaturated soil: the constitution problem (Lu and Licos 2004; Monroy et al. 2010). The MIP-predicted SWCC in this paper is not able to consider this problem.

The CAs of soils with different textures differ from each other (Woche et al. 2005). However, this study investigates Malan loess from two locations on the China Loess Plateau, and their CAs are almost the same (50° and 70° for wetting and drying, respectively). This is because the loess samples in different areas have minor variations in terms of the mineral components and texture, which implies that they may have close CA values. However, we still need more measurements and comparisons of different loess specimens to verify that the CA values are applicable for loess from different locations and depths.

5　Conclusions

All previous studies on SWCC prediction have neglected the effect of the CA on the soil matric suction, which may cause inaccuracy in the predicted curve. Therefore, a method for determining SWCC from MIP testing with consideration of the CA is proposed. Two different loess samples were tested via MIP, and their SWCCs were predicted with the proposed method and compared with PPT- and FPT-measured SWCCs. The following conclusions can be obtained:

(1) Both the study in this paper and the previous literature indicated that the CAs of hydrophilic soils are much greater than zero and have a significant effect on the SWCC. The assumption of perfect wettability (CA = 0°) of soil overestimated the SWCC and resulted in significant errors.

(2) MIP results can be used to quantitatively estimate the SWCC of loess soil by considering the CA. A good agreement between the results determined with the proposed method and the results determined by the PPT and the FPT was derived by considering an appropriate value of the CA. For loess, the wetting CA should be assumed to be 70°, and the drying CA should be assumed to be 50°.

(3) Predicting an SWCC from the MIP results requires several hours once the CA has been obtained, which saves time compared with the direct measurement methods (the tensiometer, filter paper, and axis translation methods usually take several days to a month), and only a small piece of specimen is required.

(4) The predicted SWCCs of the loess show a unimodal or bimodal form, which is consistent with the corresponding PSD curves. This result suggests that the SWCC is predominantly controlled by the pore characteristics of the soil.

However, deformation of the soil is not considered in this paper, as it involves another major problem of unsaturated soil—i.e., the constitution problem. Furthermore, more measurements and comparisons are required to clarify if CAs of 50° and 70° are applicable for all loess when predicting the SWCC using the MIP method.

Acknowledgements

References

Bachmann J, Woche SK, Goebel MO, et al. (2003) Extended methodology for determining wetting properties of porous media. Water Resources Research 39(12):11-1-11-14. https://doi.org/10.1029/2003wr002143

Diamond S (1970) Pore size distributions in clays. Clays and Clay Minerals 18(1):7-23. https://doi.org/10.1346/CCMN.1970.0180103

Dijkstra TA, Rogers CDF, Smalley IJ et al. (1994) The loess of north-central China: Geotechnical properties and their relation to slope stability. Engineering Geology 36(3-4): 153-71. https://doi.org/10.1016/0013-7952(94)90001-9

Feda J (1988) Collapse of loess upon wetting. Engineering Geology 25(2-4):263-289. https://doi.org/263-9.10.1016/0013-7952(88)90031-2

Fu H (2018) Study on Engineering Characteristics of Loess in Middle Pleistocene. Master's thesis, Chang'an University. Xi'an, China (In Chinese). https://doi.org/CNKI:CDMD:2.1018.791893

Gao GR (1979) Study of the microstructures and the collapse mechanism in loess soil from Lanzhou. Journal of Lanzhou University (6):123-134 (in Chinese). https://doi.org/10.1360/csb1980-25-20-945

Gao GR (1980) The microstructures of loess in China. Chinese Science Bulletin (20):945-8 (in Chinese). https://doi.org/CNKI:SUN:KXTB.0.1980-20-010

Goebel MO, Bachmann J, Woche SK (2008) Modified technique to assess the wettability of soil aggregates: Comparison with contact angles measured on crushed aggregates and bulk soil. European Journal of Soil Science 59(6):1241-1252. https://doi.org/10.1111/j.1365-2389.2008.01073.x

Hajnos M, Calka A, Jozefaciuk G (2013) Wettability of mineral soils. Geoderma 206:63–69. https://doi.org/10.1016/j.geoderma.2013.04.019

Kuila U, Prasad M (2013) Specific surface area and pore-size distribution in clays and shales. Geophysical Prospecting 61(2):341-362. https://doi.org/10.1111/1365-2478.12028

Lei XY (1983) Type of the loess microtextures in Xi'an district. Journal of Northwest University (4):56-65 (In Chinese). https://doi.org/CNKI:SUN:XBDZ.0.1983-04-009

Lei XY (1987) Pore types of loess soils in China and its collapsibility. Science in China: Series B (12):1310-6 (in Chinese). https://doi.org/CNKI:SUN:JBXK.0.1987-12-008

Li P, Vanapalli S, Li TL (2016) Review of collapse triggering mechanism of collapsible soils due to wetting. Journal of Rock Mechanics and Geotechnical Engineering 8(02):256-274. https://doi.org/10.1016/j.jrmge.2015.12.002

Li P, Li TL, Vanapalli SK (2018) Prediction of soil-water characteristic curve for Malan loess in Loess Plateau of China. Journal of Central South University 25(2):432-447. https://doi.org/10.1007/s11771-018-3748-1

Liu SY, Yasufuku N, Liu Q, et al. (2013a) Physically based closed-form expression for the bimodal unsaturated hydraulic conductivity function. Water Science and Technology 68(2):328-334. https://doi.org/10.2166/wst.2013.229

Liu Z, Yu X, Wan L (2013b) Influence of Contact Angle on Soil-Water Characteristic Curve with Modified Capillary Rise Method. Transportation Research Record 2349:32-40. https://doi.org/10.3141/2349-05

Lu N and Likos WJ (2004) Unsaturated Soil. Mechanics New York, PA: John Wiley & Sons, Inc. pp 449-452. http://10.1.1.57:8888/dspace/handle/hau/5179

Masrouri F, Bicalho KV, Kawai K (2008) Laboratory Hydraulic Testing in Unsaturated Soils. Geotech Geol Eng 26(6): 691-704. https://doi.org/10.1007/s10706-008-9202-7

Monroy R, Zdravkovic L, Ridley A (2010) Evolution of microstructure in compacted London Clay during wetting and loading. Géotechnique 60(2):105-119. https://doi.org/10.1680/geot.8.P.125

Muñoz-Castelblanco JA, Pereira JM, Delage P, Cui YJ (2012) The water retention properties of a natural unsaturated loess from Northern France. Geotechnique 62(2):95-106. http://dx.doi.org/10.1680/geot.9.P.084

Ng CWW, Sadeghi H, Hossen SB, et al. (2016) Water retention and volumetric characteristics of intact and re-compacted loess. Canadian Geotechnical Journal 53 (8): 1258-1269. http://doi.org/10.1139/cgj-2015-0364

Penumadu D, Dean J (2000) Compressibility effect in evaluating the pore-size distribution of kaolin clay using mercury intrusion porosimetry. Canadian Geotechnical Journal 37:393-405. https://doi.org/10.1139/cgj-37-2-393

Prapaharan S, Altschaeffl AG, Dempsey BJ (1985) Moisture Curve of Compacted Clay: Mercury Intrusion Method. Journal of Geotechnical Engineering 111(9):1139-1143. https://doi.org/10.1016/0148-9062(86)90426-2

Romero E, Gens A, Lloret A (1999) Water permeability, water retention and microstructure of unsaturated compacted Boom clay. Engineering Geology 54(1-2):117-127. https://doi.org/10.1016/S0013-7952(99)00067-8

Romero E, Simms P H (2008) Microstructure Investigation in Unsaturated Soils: A Review with Special Attention to Contribution of Mercury Intrusion Porosimetry and Environmental Scanning Electron Microscopy. Geotechnical and Geological Engineering 26(6):705-727. https://doi.org/10.1007/s10706-008-9204-5

Shang J, Flury M, Harsh JB, et al. (2008) Comparison of different methods to measure contact angles of soil colloids. Journal of Colloid and Interface Science 328(2):299-307. https://doi.org/10.1016/j.jcis.2008.09.039

Sills ID, Aylmore LAG, Quirk JP (1973) A comparison between mercury injection and nitrogen sorption as methods of determining pore size distribution. Proceedings of the Soil Science Society of America 37:535-537. https://doi.org/10.2136/sssaj1973.03615995003700040021x

Simms PH and Yanful EK (2001a) Measurement and estimation of pore shrinkage and pore distribution in a clayey till during soil-water characteristic curve tests. Canadian Geotechnical Journal 38(4):741-754. https://doi.org/10.1139/t01-014

Simms PH and Yanful EK (2001b) Predicting soil-water characteristic curves of compacted plastic soils from measured pore-size distributions. Géotechnique 52(4):269-278. https://doi.org/10.1680/geot.2002.52.4.269

Simms P H and Yanful E K (2005) A pore-network model for hydromechanical coupling in unsaturated compacted clayey soils. Canadian Geotechnical Journal 42(2): 499-514. https://doi.org/10.1139/t05-002

Sun DA, Zahng JR, Lv HB (2013) Soil-water characteristic curve of Nanyang expansive soil in full suction range. Rock and Soil Mechanics 34(7):1839-1846 (In Chinese). https://doi.org/CNKI:SUN:YTLX.0.2013-07-004

Sun JZ (2005) Loessology (Vol.1) Hong Kong Archaeological society (In Chinese).

Tan T (1988) Fundamental properties of loess from northwestern China. Engineering Geology 25(2-4): 103-22. https://doi.org/10.1016/0013-7952(88)90022-1

Wang M, Kong L, Zang M (2015) Effects of sample dimensions and shapes on measuring soil–water characteristic curves using pressure plate. Journal of Rock Mechanics and Geotechnical Engineering 7(4):463-468. https://doi.org/10.1016/j.jrmge.2015.01.002

Wang M, Pande GN, Kong LW, Feng YT (2017) Comparison of Pore-Size Distribution of Soils Obtained by Different Methods. International journal of geomechanics 17(1):1-6. https://doi.org/10.1061/(ASCE)GM.1943-5622.0000696

Washburn EW (1921) The Dynamics of Capillary Flow. Phys. rev. ser 17(3):273-283.https://doi.org/10.1103/PhysRev.17.273

Woche SK, Goebel MO, Kirkham MB, et al. (2005) Contact angle of soils as affected by depth, texture, and land management. European Journal of Soil Science 56(2):239-251. https://doi.org/10.1111/j.1365-2389.2004.00664.x

Xie WL, Li P, Zhang MS, Cheng TE, Wang Y (2018) Collapse behavior and microstructural evolution of loess soils from the Loess Plateau of China. Journal of Mountain Science 15(08):31-46. https://doi.org/10.1007/s11629-018-5006-2

Xie X (2018) Study on soil-water characteristic curve and pore characteristics of compacted loess. Master's thesis, Chang'an University. Xi'an, China (in Chinese). https://doi.org/CNKI:CDMD:2.1018.792416

Ye YX, Zou WL, Han Z, Liu XW (2019) Predicting the entire soil-water characteristic curve using measurements within low suction range. Journal of Mountain Science 16(05):255-271. https://doi.org/10.1007/s11629-018-5233-6

Zhang LM, Li X (2010) Micro Porosity Structure of Coarse Granular Soils. Journal of Geotechnical and Geoenvironmental Engineering 136(10):1425-1436. https://doi.org/10.1061/(ASCE)GT.1943-5606.0000348